Korea-Australia Rheology Journal
Vol. 13, No. 4, December 2001 pp. 205-217

Investigation of entanglement dynamics of flexible polymer chains *via* comparison of dielectric and viscoelastic properties: a review of recent findings

H. Watanabe*
Institute for Chemical Research, Kyoto University Uji, Kyoto 611-0011, Japan
(Received November 15, 2001)

Abstract

This review article summarizes results of recent viscoelastic and dielectric studies for entangled *cis*-polyisoprene (PI) chains. The PI chains have the so-called type-A dipoles parallel along the chain backbone, and their slow viscoelastic and dielectric relaxation processes reflect the same global chain motion. However, this motion is differently averaged in the viscoelastic and dielectric properties, the former representing the isochronal orientational anisotropy of individual entanglement segments while the latter detecting the orientational correlation of the segments at two separate times (0 and t). On the basis of this difference, the viscoelastic and dielectric data of the entangled PI chains were compared to elucidate detailed features of the chain dynamics. Specifically, the molecular picture of dynamic tube dilation (DTD) incorporated in recent models was tested for linear and star PI chain. The comparison revealed that the DTD picture was valid for linear PI chains but failed for the star PI chains in the dominant part of the terminal relaxation. The failure for the star chains was related to the pre-requisite for the DTD process, rapid equilibration of successive entanglement segments through their constraint release (CR) motion: For the star chains, the dilated tube diameter expected in the terminal regime was considerably large because of a broad distribution of motional modes of the chains, so that the CR-equilibration required for DTD could not occur in time. The terminal relaxation of the star chain appeared to occur through the CR process before the expected DTD process was completed. The situation was different for the linear chain exhibiting narrowly distributed motional modes. The dilated tube expected for the linear chain was rather thin and the required CR-equilibration occurred in time, resulting in the success of the DTD picture. These detailed features of the chain dynamics was revealed only when the viscoelastic and dielectric properties were compared, demonstrating the importance of this comparison.

1. Introduction

Entanglement is the most prominent feature of long flexible chains (Ferry, 1980; Doi and Edwards, 1986; Watanabe, 1999). The entanglement represents a constraint for large scale (global) motion of mutually uncrossable chains. The global motion is insensitive to the chemical structure of the chains but strongly affected by the topological structure (e.g., long-chain branching), and all kinds of slow relaxation phenomena result from this motion. Thus, extensive studies have been made for various dynamic properties to reveal several interesting features such as the exponential retardation of the relaxation of star-branched chains with increasing arm length.

However, we should note that the thermal motion of the chains has a stochastic nature and any dynamic property obtained from macroscopic measurements detects the time evolution of the chain conformation *averaged in a way intrinsic to the property*: For example, the linear viscoelastic property detects the averaged orientational anisotropy of the chains that decays with time through the chain motion (Doi and Edwards, 1986; Watanabe, 1999). In other words, details of this motion cannot be uniquely specified only from a knowledge about any *single* property.

Experimentally, such details have been examined through comparison of various properties that differently average the chain conformation, e.g., viscoelastic, optical, dielectric, and diffusion properties (Tassin *et al.*, 1988; Lantman *et al.*, 1989; Ylitalo *et al.*, 1990; Bartles *et al.*, 1986; Shull *et al.*, 1988; Watanabe *et al.*, 1996, 1998, 2000; Matsumiya *et al.*, 2000, 2001; Watanabe, 2001). In fact, the comparison revealed several interesting features, for example, a difference in the diffusion and viscoelastic relaxation times for entangled star chains (Bartles *et al.*, 1986; Shull *et al.*, 1988), partial coherence in motion of submolecules in the linear chain due to entanglement (Watanabe *et al.*, 1996, 1998), and validity/failure of a particular molecular picture

*Corresponding author: hiroshi@scl.kyoto-u.ac.jp

referred to as *dynamic tube dilation* (*DTD*; Marrucci, 1985; Ball and McLeish, 1989; Milner and McLeish, 1997, 1998) found for entangled linear/star chains (Matsumiya *et al.*, 2000, 2001; Watanabe *et al.*, 2000, 2001).

This review article focuses its attention on the validity/failure of the DTD picture deduced from comparison of the viscoelastic and dielectric properties, thereby demonstrating the importance of this comparison. In section 2, these properties of the so-called type-A chains having electrical dipoles parallel along the chain backbone are expressed in terms of the chain conformation. Then, in section 3, the DTD molecular picture is briefly explained in relation to these expressions. Section 4 presents the viscoelastic and dielectric data of representative type-A chains, linear and star *cis*-polyisoprene (PI) chains. The DTD molecular picture is tested through comparison of these data. Finally, section 5 gives a summary of this article.

2. Molecular expression of viscoelastic and dielectric properties

Fig. 1 schematically shows monodisperse linear and star chains examined in this article. The linear chain is composed of N entanglement segments (indicated with circles), and each star-arm has N_a entanglement segments. This segment, having the molecular weight M_e, is the motional unit during the entanglement relaxation at long times. The short, solid arrows indicate the bond vectors (end-to-end vectors) of these segments, $\boldsymbol{u}(n, t)$ and/or $\boldsymbol{u}_\alpha(n, t)$ where n and α are the segment and arm indices (the latter being defined only for the star chain). This bond vector, having the average length a at equilibrium, is the structural quantity that relates the viscoelastic/dielectric properties to the chain motion.

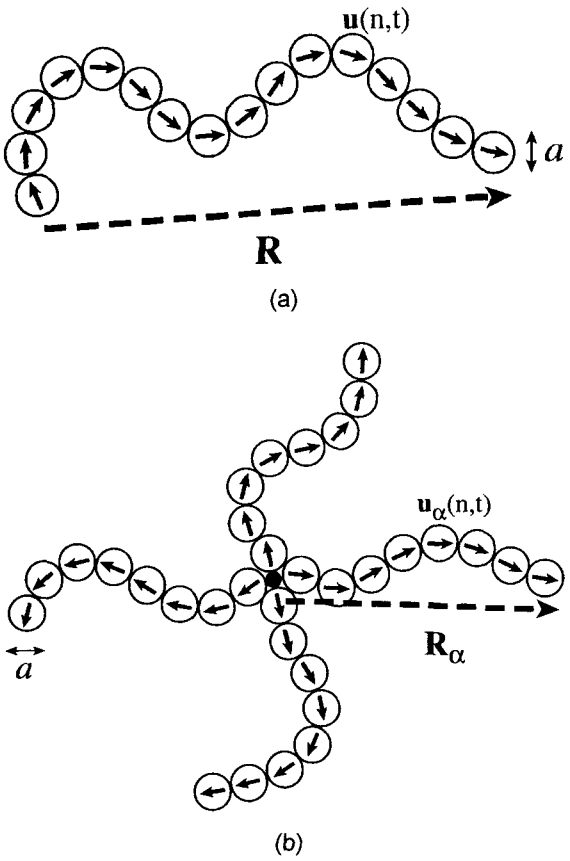

Fig. 1. Schematic illustration of type-A linear and star chains. The circles indicate the entanglement segments of the size a having the bond vectors $\boldsymbol{u}$ (short solid arrows). The dipole of the segment is parallel to this $\boldsymbol{u}$.

2.1. Viscoelastic property

For flexible chains in long time scales, extensive experiments establish the stress-optical rule, i.e., the proportionality between the stress and orientational anisotropy of the chain (Janeschitz-Kriegl, 1983; Ferry, 1980; Doi and Edwards, 1986). For the entangled linear and q-arm star chains subjected to a small step shear strain γ at $t = 0$, this rule allows us to express the normalized relaxation modulus $\mu(t)=G(t)/G_N$ (G_N=entanglement plateau modulus) in terms of the segment bond vector $\boldsymbol{u}$:

$$\mu(t) = \frac{1}{S_0 N} \sum_{n=1}^{N} \frac{1}{a^2} \langle u_x(n,t) u_y(n,t) \rangle \quad \text{for linear chain} \tag{1}$$

$$\mu(t) = \frac{1}{S_0 N_a q} \sum_{\alpha=1}^{q} \sum_{n=1}^{N_a} \frac{1}{a^2} \langle u_{\alpha,x}(n,t) u_{\alpha,y}(n,t) \rangle \quad \text{for q-arm star chain} \tag{2}$$

Here, x- and y-directions are chosen as the shear and shear gradient directions, respectively, and the subscript ξ (= x, y) stands for the ξ-component of $\boldsymbol{u}$.

As noted from Eqs. (1) and (2), the modulus is determined by the isochronal orientational anisotropy of individual entanglement segments, $\langle u_x u_y \rangle / a^2$. The normalization constant S_0 represents the initial anisotropy given by

$$S_0 = \gamma / 3 \quad \text{for affine deformation} \tag{3}$$

If we utilize the Doi-Edwards initial condition, S_0 is modified to $4\gamma/15$. However, the modulus expression and the corresponding argument in this article are not affected by the difference in the S_0 values for these conditions.

In most of experiments, linear viscoelastic behavior of entangled polymers is tested under oscillatory strain. The normalized storage and loss moduli at angular frequency ω, characterizing this behavior, are related to $\mu(t)$ through the Fourier transformation (Ferry, 1980):

$$\frac{G'(\omega)}{G_N} = \omega \int_0^\infty \mu(t) \sin \omega t \, dt \,, \quad \frac{G''(\omega)}{G_N} = \omega \int_0^\infty \mu(t) \cos \omega t \, dt \tag{4}$$

Thus, the ω dependence of these moduli reflects the distribution of the orientational relaxation modes (averaged in μ).

2.2. Dielectric property

In general, slow dielectric relaxation detects thermal fluctuation of the electrical polarization $\boldsymbol{P}(t)$, and the normalized dielectric relaxation function $\Phi(t)$ is given by the autocorrelation $\langle \boldsymbol{P}(t) \cdot \boldsymbol{P}(0) \rangle / \langle \boldsymbol{P}^2 \rangle$ (Riande and Saiz, 1992; Watanabe, 2001). The so-called type-A chains of our interest have the dipoles *parallel* to the bond vector $\boldsymbol{u}$ of the segments (cf. Fig. 1). For these chains, the global motion induces the fluctuation of $\boldsymbol{P}$ and is dielectrically detectable.

Specifically, for the linear chain having the *non-inverted* dipoles, $\boldsymbol{P}(t)$ is proportional to a sum $\sum_{n=1}^{N} \boldsymbol{u}(n,t)$ ($=\boldsymbol{R}(t)$; end-to-end vector shown in Fig. 1a). The $\Phi(t)$ of this chain is expressed as (Watanabe, 1999, 2001)

$$\Phi(t) = \frac{1}{N} \sum_{n,n'=1}^{N} \frac{1}{a^2} \langle \boldsymbol{u}(n,t) \cdot \boldsymbol{u}(n',0) \rangle = \frac{1}{Na^2} \langle \boldsymbol{R}(t) \cdot \boldsymbol{R}(0) \rangle$$

(for linear chain) (5)

Similarly, for the star chain having the parallel dipoles in each arm that are once inverted at the branching point, we find (Watanabe *et al.*, 2000)

$$\Phi(t) = \frac{1}{qN_a a^2} \sum_{\alpha,\alpha'=1}^{q} \langle \boldsymbol{R}_\alpha(t) \cdot \boldsymbol{R}_{\alpha'}(0) \rangle$$

(for q-arm star chain) (6)

Here, R_α is the vector connecting the branching point and the end of α-th arm (cf. Fig. 1b).

The dynamic dielectric constant $\varepsilon'(\omega)$ and dielectric loss $\varepsilon''(\omega)$ at angular frequency ω, the most frequently measured quantities, are related to $\Phi(t)$ as (Riande and Saiz, 1992).

$$\frac{\varepsilon_0 - \varepsilon'(\omega)}{\Delta\varepsilon} = \omega \int_0^\infty \Phi(t) \sin \omega t \, dt, \quad \frac{\varepsilon''(\omega)}{\Delta\varepsilon} = \omega \int_0^\infty \Phi(t) \cos \omega t \, dt \tag{7}$$

Here, ε_0 is the static dielectric constant and $\Delta\varepsilon$ is the dielectric relaxation intensity (for the global chain motion). Thus, the ω dependence of $\{\varepsilon_0 - \varepsilon'(\omega)\}/\Delta\varepsilon$ and $\varepsilon''/\Delta\varepsilon$ reflects the mode distribution of orientational correlation decay (averaged in Φ).

For $\Phi(t)$, this mode distribution is conveniently expressed in terms of a (discretized) dielectric spectrum $\{g_p, \tau_p\}$; $\Phi(t) = \sum_{p \geq 1} g_p \exp[-t/\tau_p]$ (Watanabe, 2001). Here, g_p represents the normalized intensity of p-th dielectric mode having the relaxation time τ_p; τ_p is defined in the order $\tau_1 > \tau_2 > \tau_3$, ..., and the intensities satisfy a relationship, $\sum_{p \geq 1} g_p = \Phi(0) = 1$. Correspondingly, $\varepsilon'(\omega)$ and $\varepsilon''(\omega)$ are expressed in terms of $\{g_p, \tau_p\}$ as

$$\frac{\varepsilon_0 - \varepsilon'(\omega)}{\Delta\varepsilon} = \omega^2 \sum_{p \geq 1} g_p \frac{\tau_p^2}{1 + \omega^2 \tau_p^2}, \quad \frac{\varepsilon''(\omega)}{\Delta\varepsilon} = \omega \sum_{p \geq 1} g_p \frac{\tau_p}{1 + \omega^2 \tau_p^2} \tag{8}$$

2.3. Differences between dielectric and viscoelastic properties

Comparing Eqs. (1), (2), (5), and (6), we note an important difference between the viscoelastic and dielectric properties. The viscoelastic $\mu(t)$ detects the *isochronal* orientational anisotropy of *individual* segments, while the dielectric $\Phi(t)$ reflects the orientational correlation of any *two* segments at *separate* times (t and 0). Thus, the same stochastic motion of the chain is differently averaged in $\mu(t)$ and $\Phi(t)$, meaning that a relationship between the dielectric and viscoelastic properties changes with the type of chain dynamics. (For example, reptating linear chains have $\mu(t) = \Phi(t)$ while Rouse chains have $\mu(t) \neq \Phi(t)$; Watanabe, 1999) This difference between the viscoelastic and dielectric properties is a key in our experimental test of the dynamic tube dilation (DTD) mechanism.

3. DTD molecular picture

In entangled systems, large scale motion of a particular chain (probe chain) is constrained by the surrounding chains (matrix chains). In early models assuming immobile constraints, the probe motion is effectively limited in a *spatially fixed* tube-like region surrounding the probe backbone (Doi and Edwards, 1978; Pearson and Helfand, 1984). In these models, the probe motion over distances larger than the tube diameter a (= entanglement mesh size) is allowed only along the curvilinear axis of the tube. The equation motion of this probe can be solved to give the time evolution of the orientational anisotropy $\langle u_x(n,t) u_y(n,t) \rangle / a^2$ and orientational correlation $\langle \boldsymbol{u}(n,t) \cdot \boldsymbol{u}(n',0) \rangle / a^2$, from which the viscoelastic and dielectric properties are readily calculated through Eqs. (1)-(8).

The prediction of the fixed tube model is in qualitative agreement with experiments, suggesting the fundamental validity of the concept of topological constraint represented by the tube. However, quantitative differences between the calculated and observed properties, such as the well known difference between the calculated and measured relaxation times of linear chains (being proportional to N^3 and $N^{3.5\pm0.2}$, respectively), indicate necessity of refinement of the model.

The motion allowed for the probe chain can occur, in principle, also for the matrix chains, in particular in the monodisperse systems where the probe and matrix are identical to each other. This matrix motion naturally results in the deformation/motion of the tube. Thus, the tube model has been refined mainly by incorporating the tube motion into the model.

The tube motion activates two different (but intimately related) mechanisms of the probe relaxation, the *constraint release* (CR) mechanism (Klein, 1978; Graessley, 1982) and *dynamic tube dilation* (DTD) mechanism (Marrucci, 1985, Ball and McLeish, 1989; Milner and McLeish, 1997,

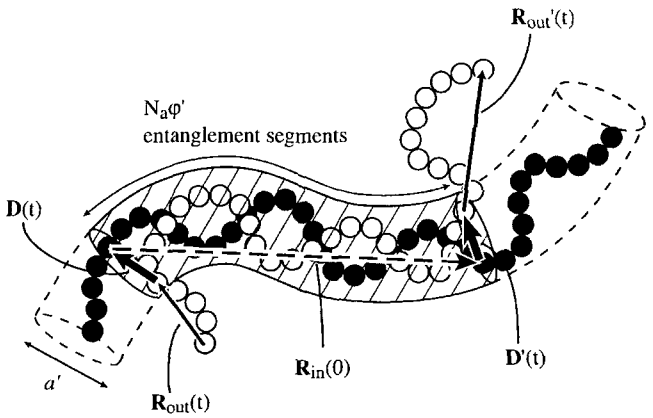

Fig. 2. Schematic illustration of a linear chain in a dilated tube. Filled and unfilled circles indicate the entanglement segments at times 0 and t.

1998). The CR mechanism allows each entanglement segment of the probe to laterally jump over distances > a, and accumulation of such local CR jumps results in the global CR relaxation (Graessley, 1982). This global CR relaxation process approximately obeys the retarded Rouse-dynamics, as revealed from extensive experiments for binary blends (Watanabe, 1999).

In the DTD mechanism, the tube dilates to an extent determined by the fractional memory of the initial chain orientation, and the chain moves along the dilated tube. Under an assumption about the dilated tube diameter, we can calculate the viscoelastic $\mu(t)$ and dielectric $\Phi(t)$ of the chains and derive a particular relationship between $\mu(t)$ and $\Phi(t)$ for the DTD relaxation process. These expressions and relationships are summarized below.

3.1. DTD expression of $\mu(t)$

We consider the type-A linear chain that is composed of N entanglement segments and constrained in a dilated tube of the diameter a'. In Fig. 2, the entanglement segments of this chain at times 0 and t are shown with the filled and unfilled circles, respectively. Every successive β (= $\{a'/a\}^2$) segments *at the time 0* are coarse-grained into an enlarged segment, and the dilated tube is defined as an envelope of these enlarged segments. At the time t, the surviving portion of this tube (indicated with hatching) constrain some number (N_t) of the entanglement segments. The *average* survival fraction of the dilated tube is defined as a fraction of these constrained entanglement segments, $\varphi' = N_t / N$.

The DTD process occurs as a result of the CR-equilibration over the successive β segments. As explained in Appendix A, the modulus decays by the factor of $1/\beta$ due to this equilibration. Thus, the normalized modulus is given by $\mu(t) = \varphi'(t)/\beta$ when the fraction $\varphi'(t)$ of the entanglement segments are constrained in the dilated tube.

This $\mu(t)$ is rewritten under an assumption that the relaxed segments behave as a solvent and the bulk polymer system is equivalent to a solution with the polymer volume fraction $\varphi'(t)$ (Marrucci, 1985). For this case, the dilated tube diameter (= effective entanglement mesh size in this solution) is evaluated as $a' = a\{\varphi'(t)\}^{-d/2}$ and β (= $\{a'/a\}^2$) is given by $\{\varphi'(t)\}^{-d}$, where the dilation exponent d is in a range between 1 and 1.3 (as observed for usual solutions; Ferry, 1980). Then, we find

$$\mu(t) = \{\varphi'(t)\}^{1+d} \text{ for DTD process} \tag{9}$$

This DTD expression of $\mu(t)$ was firstly derived by Marrucci (1985).

For the star chains, we can similarly define the dilated tube to derive an expression of $\mu(t)$. It turns out that this expression is also given by Eq. (9) (Watanabe *et al.*, 2000). This result is naturally expected because Eq. (9) is derived from an argument of the modulus decay due to the CR-equilibration without specific assumptions about the chain motion in the dilated tube.

3.2. DTD expression of $\Phi(t)$

Here, we derive an expression of the dielectric $\Phi(t)$ of the linear type-A chain. For this purpose, the end-to-end vector $\boldsymbol{R}(t)$ of the chain at the time t is conveniently subdivided into three vectors, $\boldsymbol{R}_{out}(t)$ and $\boldsymbol{R}_{out}'(t)$ of the two outer portions having escaped from the dilated tube and $\boldsymbol{R}_{in}(t)$ for the inner portion remaining in the surviving portion of this tube; see Fig. 2. The outer portions are randomized and their $\boldsymbol{R}_{out}(t)$ and $\boldsymbol{R}_{out}'(t)$ are not correlated with the initial configuration $\boldsymbol{R}(0)$, while the inner portion partly preserves the correlation. Thus, Eq. (5) is rewritten as $\Phi(t) = \langle \boldsymbol{R}_{in}(t) \cdot \boldsymbol{R}_{in}(0) \rangle / Na^2$, where $\boldsymbol{R}_{in}(0)$ is the end-to-end vector of the inner portion at the time *0* that is included in the surviving portion of the dilated tube at the time t; cf. thin dashed arrow in Fig. 2.

The $\boldsymbol{R}_{in}(t)$ is further subdivided as $\boldsymbol{D}(t) + \boldsymbol{D}'(t) + \boldsymbol{R}_{in}(0)$, where $\boldsymbol{D}(t)$ and $\boldsymbol{D}'(t)$ represent displacements in the two edge planes of the surviving portion of the dilated tube; see thick solid arrows. This displacement is defined as a difference of the positions of the segments *at times 0 and t* located somewhere in a given edge of this portion.

After the above subdivision of $\boldsymbol{R}_{in}(t)$, $\Phi(t)$ is further rewritten in a form:

$$\Phi(t) = \varphi'(t) + \frac{1}{Na^2}[\langle \boldsymbol{D}(t) \cdot \boldsymbol{R}_{in}(0) \rangle + \langle \boldsymbol{D}'(t) \cdot \boldsymbol{R}_{in}(0) \rangle] \tag{10}$$

where we have utilized an identity $\langle \{\boldsymbol{R}_{in}(0)\}^2 \rangle = Na^2\varphi'(t)$ reflecting the Gaussian nature of the chain. Eq. (10) indicates that the displacements in the edges of the surviving portion of the dilated tube may affect the dielectric relaxation (through the second term).

This *tube-edge effect* vanishes *if* the time scale of our observation is well below a time $\tau_{eq,in}$ required for equilibration of both length (| $\boldsymbol{R}_{in}$ |) and orientation ($\boldsymbol{R}_{in}$/| $\boldsymbol{R}_{in}$ |) of

the inner portion. In this time scale, the displacements $\boldsymbol{D}(t)$ and $\boldsymbol{D}'(t)$ would be random and uncorrelated with the initial configuration, and Eq. (10) is simplified to

$$\Phi(t) = \varphi'(t) \text{ for } t < \tau_{eq,in} \quad \text{(in absence of the tube edge-effect)} \tag{11}$$

This DTD expression of $\Phi(t)$ was firstly derived by Matsumiya *et al.* (2000) without specifying the time scale of its validity.

Rigorously speaking, the orientational equilibration of the inner portion is completed only when the chain escapes from the dilated tube. Thus, $\tau_{eq,in}$ should be close to the longest relaxation time τ_{max}. However, some degree of equilibration may occur even at $t < \tau_{eq,in}$, and Eq. (11) may need to be modified accordingly (by retaining the second term in Eq. (10)). The largest modification is made when the full equilibration is assumed. For this case, we find (cf. Appendix B):

$$\Phi(t) = \varphi'(t) - \frac{1}{4N}[\{\varphi'(t)\}^{-d/2} - 1]^2 \tag{12}$$

for linear chain in presence of maximum tube-edge effect

Now, we turn our attention to the q-arm star chains with each arm being composed of N_a entanglement segments (Fig. 1b). In absence of the tube-edge effect, $\Phi(t)$ of this star chain is also given by Eq. (11) (Watanabe *et al.*, 2000). In presence of this effect, $\Phi(t)$ is expressed in terms of the tube survival fraction $\varphi'(t)$ as (Watanabe *et al.*, 2001)

$$\Phi(t) = \varphi'(t) - \frac{1}{8N_a}[\{\varphi'(t)\}^{-d/2} - 1]^2 \tag{13}$$

for star chain in presence of maximum tube-edge effect

In derivation of Eq. (13), we followed the tube model to assume the immobile branching point. (Each star arm has one edge plane of the dilated tube where the tube-edge effect emerges, while the linear chain has two edge-planes. This difference led to a difference between the prefactors 1/4 N and 1/8N_a appearing in Eqs. (12) and (13).)

It should be emphasized that Eqs. (12) and (13) overestimate the tube-edge effect because the assumed orientational equilibration of the chain in the surviving tube portion is completed only at $t \sim \tau_{max}$. This effect (represented by the second term in Eqs. (12) and (13)) becomes important at long t where $\varphi'(t)$ decays to $O(N^{-1/(1+d)})$ thereby giving comparable magnitudes of the φ' and $\{\varphi'\}^{-d}/N$ factors.

3.3. DTD relationship between $\mu(t)$ and $\Phi(t)$

As noted from Eqs. (9) and (11)-(13), $\mu(t)$ and $\Phi(t)$ satisfy a particular relationship(s) if the DTD molecular picture is valid. Specifically, in absence of the tube-edge effect, this relationship is written in a very simple form:

$$\mu(t) = \{\Phi(t)\}^{1+d} \text{ for both linear and star chains in absence of tube-edge effect} \tag{14}$$

This relationship, as well as the DTD relationship in presence of the tube-edge effect, can be tested by comparing the viscoelastic and dielectric data of the linear/star type-A chains.

3.4. Milner-McLeish model for star chains

We derived the above DTD relationship(s) without specifying the type of the chain motion along the dilated tube. In other words, the functional form (t dependence) of $\mu(t)$ and $\Phi(t)$ is not specified in the relationship(s). This form can be obtained from detailed molecular models, for example, the Marrucci model (1985) for the linear chain and Ball-McLeish (BM; 1989) and Milner-McLeish (MM; 1997, 1998) models for the star chain. For convenience of later discussion, the explicit form of $\mu(t)$ and $\Phi(t)$ deduced from the most elaborated MM model is summarized below.

In the MM model (with the dilation exponent $d = 4/3$), the star arm relaxes *via* shallow Rouse-like fluctuation at short t and *via* deep retraction along the dilated tube at long t. This retraction is associated with an entropic barrier U_{MM} and exponentially retarded with increasing retraction depth. Thus, in the MM model, each entanglement segment has a well-defined relaxation time $\tau_{MM}(z)$ determined by its curvilinear coordinate z (that coincides with the retraction depth required for the relaxation of this segment). This $\tau_{MM}(z)$ is written as (Milner and McLeish, 1997, 1998)

$$\tau_{MM}(z) \cong \frac{\tau_{sh}(z)\exp\left(\frac{U_{MM}(z)}{k_BT}\right)}{1+\frac{\tau_{sh}(z)}{\tau_{dp}(z)}\exp\left(\frac{U_{MM}(z)}{k_BT}\right)} \tag{15}$$

where $\tau_{sh}(z)$ and $\tau_{dp}(z)$ are the characteristic times for the shallow fluctuation and deep retraction,

$$\tau_{sh}(z) = \frac{225\pi^3\tau^* N_a^4}{256}\left(\frac{z}{L_{eq}}\right)^4 \tag{16}$$

and

$$\tau_{dp}(z) \cong \frac{\tau^* N_a^{3/2}\pi^{5/2}\exp\left(\frac{U_{MM}(z)}{k_BT}\right)}{30^{1/2}\left(\frac{z}{L_{eq}}\right)\left[\left\{1-\frac{z}{L_{eq}}\right\}^{8/3} + \Gamma\left(\frac{3}{7}\right)^{-2}\left(\frac{28}{45N_a}\right)^{8/7}\right]^{1/2}} \tag{17}$$

with

$$U_{MM}(z) = \frac{27N_ak_BT}{56}\left[1-\left(1-\frac{z}{L_{eq}}\right)^{7/3}\left(1+\frac{7z}{3L_{eq}}\right)\right] \tag{18}$$

In Eqs. (15)-(18), L_{eq} (= aN_a) represents the equilibrium arm length, τ^* corresponds to the Rouse relaxation time in one entanglement segment, and k_B and T are the Boltzmann constant and absolute temperature, respectively.

In formulation of $\mu(t)$ and $\Phi(t)$ of the MM model, we consider a *conditional* tube survival fraction $\tilde{\varphi} = 1 - z/L_{eq}$ for a given retraction depth z, not the average fraction φ utilized in Eqs. (9)-(13). The conditional viscoelastic memory defined for this retraction is given by $\tilde{\mu} = (1 - z/L_{eq})^{7/3}$; cf. Eq. (9) with φ being replaced by $\tilde{\varphi}$. Similarly, the conditional dielectric memory is given by $\tilde{\Phi} = 1 - z/L_{eq}$ and $\tilde{\Phi} = 1 - z/L_{eq} - \{(1 - z/L_{eq}\}^{-2/3} - 1\}^2/8N_a$ in absence and presence of the tube-edge effect, respectively; cf. Eqs. (11) and (13) with φ being replaced by $\tilde{\varphi}$. The memories sustained by the segments located between z and $z + dz$, $|\, d\tilde{\mu}/dz \,|\, dz$ and $|\, d\tilde{\Phi}/dz \,|\, dz$, decay with the relaxation time $\tau_{MM}(z)$. Thus, the $\mu(t)$ and $\Phi(t)$ deduced from the MM model are written as (Milner and McLeish, 1997, 1998; Watanabe *et al*, 2001)

$$\mu(t) = \frac{7}{3L_{eq}}\int_0^{L_{eq}}\left[1-\frac{z}{L_{eq}}\right]^{4/3}\exp\left(-\frac{t}{\tau_{MM}(z)}\right)dz$$

with/without tube-edge effect (19)

and

$$\Phi(t) = \frac{1}{L_{eq}}\int_0^{L_{eq}}\exp\left(-\frac{t}{\tau_{MM}(z)}\right)dz$$

in absence of tube-edge effect (20)

or

$$\Phi(t) = \frac{1}{K_n L_{eq}}\int_0^{z_c}\left[1+\frac{1}{6N_a}\left\{\left(1-\frac{z}{L_{eq}}\right)^{-7/3}-\left(1-\frac{z}{L_{eq}}\right)^{-5/3}\right\}\right] \times\exp\left(-\frac{t}{\tau_{MM}(z)}\right)dz$$

in presence of tube-edge effect (21)

with

$$z_c = L_{eq} - a \quad \text{and} \quad K_n = \frac{z_c}{L_{eq}} + \frac{1}{8N_a}\left[1-\left(1-\frac{z_c}{L_{eq}}\right)^{-2/3}\right]^2 \qquad (22)$$

In Eq. (21), the upper bound of the integral z_c is introduced to avoid divergence of the integral. (The full relaxation can be achieved when the arm retracts by a distance L_{eq} - a, and this distance is chosen as z_c.) The K_n is a normalization factor ensuring $\Phi(0) = 1$.

At t well below the longest relaxation time τ_{max}, the $\mu(t)$ and $\Phi(t)$ deduced from the MM model (Eqs. (19) and (20)) satisfy the DTD relationship derived on the basis of the average φ, Eq. (14) with $d = 4/3$. However, deviation from Eq. (14) is noted at $t \sim \tau_{max}$ because the conditional $\tilde{\varphi}$ is utilized in the model. (Instead, the $\Phi(t)$ given by Eq. (20) is numerically close to $\{\mu(t)\}^2$ in the entire range of $t \le \tau_{max}$ and Eq. (14) with $d = 1$ holds as a good approximation for the MM model; Watanabe *et al.*, 2001.) Eqs. (19)-(21) are later utilized to test of the DTD picture for the star chain.

4. Results and Discussion

4.1. overview

For monodisperse linear and 6-ram star *cis*-polyisoprene (PI) chains, respectively, Figs. 3 and 4 show angular frequency (ω) dependence of the normalized dynamic dielectric constant $\{\varepsilon_0 - \varepsilon'\}/\Delta\varepsilon$ and dielectric loss $\varepsilon''/\Delta\varepsilon$. The numbers indicate the entanglement density, $N = M/M_e$ and/or $N_a = M_{arm}/M_e$, where M_e (= 5×10^3 for bulk PI) is the molecular weight of the entanglement segment. The time temperature superposition worked excellently for these dielectric data (with the shift factor a_T identical to that for the viscoelastic moduli), and the data were reduced at 40°C.

The linear PI chains have non-inverted type-A dipoles, and the star PI chains have the dipoles once inverted at the branching point; see Fig. 1. For these chains, the slow dielectric relaxation seen in Figs. 3 and 4 is exclusively attributed to the global motion that is retarded with increasing N and/or N_a. (At 40°C, the local relaxation due to motion of monomeric segments emerges at high ω (> 10^7 s^{-1}) not covered in our experiments; Watanabe, 2001).

At sufficiently low ω, the linear/star PI chains exhibit the terminal tails characterizing completion of the global dielectric relaxation, $\{\varepsilon_0 - \varepsilon'\} \propto \omega^2$ and $\varepsilon'' \propto \omega$ (cf. Eq. (8)). From these tails, the second-moment average relaxation time is evaluated as

$$\langle\tau_\varepsilon\rangle_w = \frac{[(\varepsilon_0-\varepsilon')/\omega^2]_{\omega\to 0}}{[\varepsilon''/\omega]_{\omega\to 0}} = \frac{\sum_{p\ge 1} g_p\tau_p^2}{\sum_{p\ge 1} g_p\tau_p} \qquad (23)$$

This $\langle\tau_\varepsilon\rangle_w$ is related to the dielectric spectrum $\{g_p, \tau_p\}$ in a well-defined way (Eq. (23)) and can be utilized as the dielectric terminal relaxation time (Watanabe, 2001). In fact, $\langle\tau_\varepsilon\rangle_w$ is analogous to the viscoelastic terminal relaxation time $\langle\tau_G\rangle_w$ that is evaluated from the low ω tails of storage and loss moduli ($G' \propto \omega^2$ and $G'' \propto \omega$) and related to the viscoelastic spectrum $H(\tau)$ (Ferry, 1980),

$$\langle\tau_G\rangle_w = \frac{[G'/\omega^2]_{\omega\to 0}}{[G''/\omega]_{\omega\to 0}} = \frac{\int_{-\infty}^{\infty} H(\tau)\tau^2 d\ln\tau}{\int_{-\infty}^{\infty} H(\tau)\tau\, d\ln\tau} \qquad (24)$$

For the entangled PI chains examined in Figs. 3 and 4, Fig. 5 shows plots of $\langle\tau_\varepsilon\rangle_w$ (unfilled symbols) and $\langle\tau_G\rangle_w$ (filled symbols) against the span length $2N_a$ (for the star PI) and/or N (for the linear PI). For both star and linear PI, $\langle\tau_\varepsilon\rangle_w$ is close to $\langle\tau_G\rangle_w$. This result confirms that the dielectric and viscoelastic relaxation processes detect the same global chain motion.

Figs. 3-5 clearly demonstrate differences between the star and linear chains. As noted in Fig. 5, $\langle\tau_\varepsilon\rangle_w$ of the entangled linear chains increases in proportion to $N^{3.5\pm0.1}$ while the

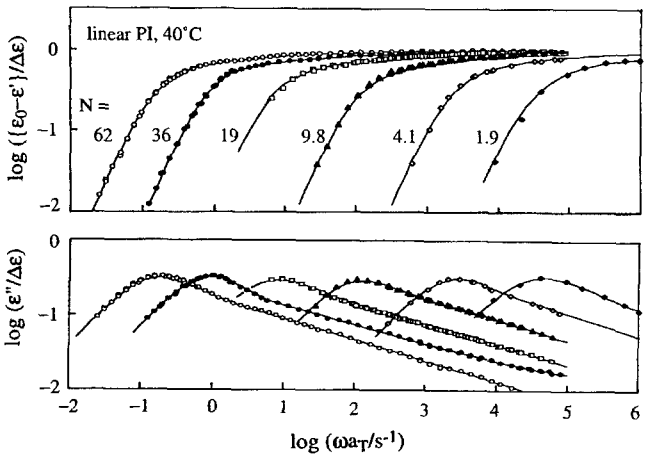

Fig. 3. Normalized dielectric constant $\{\varepsilon_0 - \varepsilon'\}/\Delta\varepsilon$ and dielectric loss $\varepsilon''/\Delta\varepsilon$ of linear PI chains with various entanglement densities N ($= M/M_e$). These chains have non-inverted type-A dipoles. The data were taken from Yoshida *et al.* (1989), Matsumiya *et al.* (2000), and Watanabe *et al.* (1998, 2001).

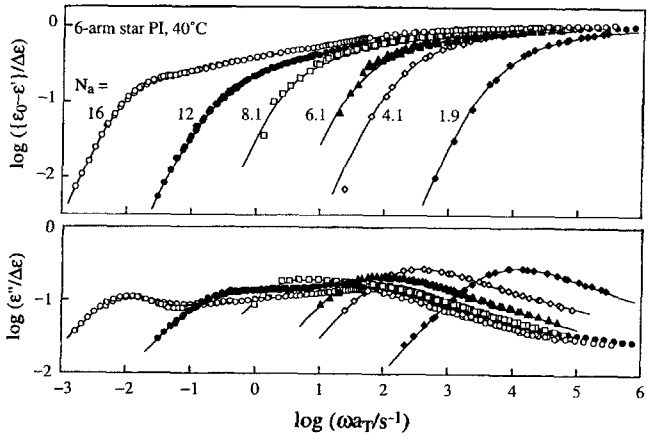

Fig. 4. Normalized dielectric constant $\{\varepsilon_0 - \varepsilon'\}/\Delta\varepsilon$ and dielectric loss $\varepsilon''/\Delta\varepsilon$ of 6-arm star PI chains with various entanglement densities N_a ($= M_a/M_e$). These star PI chains have the dipoles once inverted at the branching point. The data were taken from Yoshida *et al.* (1989) and Watanabe *et al.* (2000, 2001).

well-entangled star chains exhibit much stronger, exponential N_a dependence of $<\tau_\varepsilon>_w$. This difference has been well known for the viscoelastic $<\tau_G>_w$ (Ferry, 1980; Watanabe, 1999) and Fig. 5 confirms the same difference dielectrically.

A more important difference is noted for the dielectric mode distribution of the linear and star chains. For the linear PI chains, this distribution (observed as the ω dependence of $\{\varepsilon_0 - \varepsilon'\}/\Delta\varepsilon$ and $\varepsilon''/\Delta\varepsilon$) is insensitive to N; see Fig. 3. In contrast, for the star PI chains, the dielectric mode distribution significantly broadens with increasing N_a (cf.

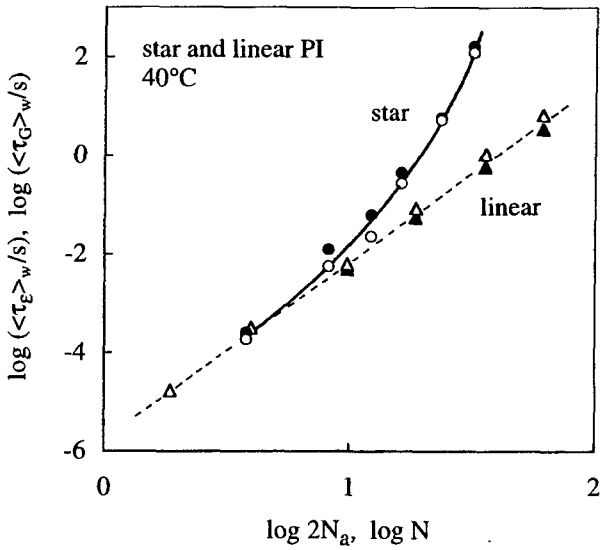

Fig. 5. Dielectric and viscoelastic terminal relaxation times, $<\tau_\varepsilon>_w$ (unfilled symbols) and $<\tau_G>_w$ (filled symbols), of entangled, linear and 6-arm star PI chains at 40°C. These times are plotted against $2N_a$ (for PI stars) and/or N (for linear PI chains). The data were taken from Yoshida *et al.* (1989), Matsumiya *et al.* (2000), and Watanabe *et al.* (1998, 2000, 2001).

Fig. 4).

Concerning this dielectric mode distribution of the star PI chains, we note two broad peaks in the $\varepsilon''/\Delta\varepsilon$ curve for $N_a \geq 12$; see Fig. 4. This result indicates that the highly entangled star PI chains exhibit well separated fast and slow (terminal) dielectric relaxation processes. Viscoelastic G'' of highly entangled stars exhibits a similar high-ω peak corresponding to the fast process (Fetters *et al.*, 1993), with an example being seen later in Fig. 6. This high-ω peak of G'' is assigned to the Rouse-like fluctuation of the arm length. Thus, the fast dielectric process seen as the $\varepsilon''/\Delta\varepsilon$ peak at $\omega a_T = 50 - 100$ s^{-1} (for $N_a = 12$ and 16) is also attributable to this fluctuation.

The separation between this fluctuation process and the terminal relaxation process rapidly decreases with decreasing N_a (< 12) because of the exponential N_a dependence of $<\tau_\varepsilon>_w$ (Fig. 5). Thus, for the star PI with N_a = 8.1, the fast fluctuation process is not observed as a well-resolved $\varepsilon''/\Delta\varepsilon$ peak but as a shoulder at $\omega a_T \cong 200$ s^{-1}; cf. Fig. 4. For smaller N_a (≤ 6.1), the fast and terminal processes merge with each other to give a single broad $\varepsilon''/\Delta\varepsilon$ peak.

As noted in Fig. 4, the peak/shoulder of $\varepsilon''/\Delta\varepsilon$ (for $N_a \geq 8.1$) assigned to the arm length fluctuation shifts to lower ω with increasing N_a. This shift is consistent with the $N_a^{-2.6}$ dependence of the G'' peak frequency reported for well-entangled star PI chains (Fetters *et al.*, 1993).

In contrast, the terminal viscoelastic/dielectric relaxation of the entangled stars is exponentially retarded with

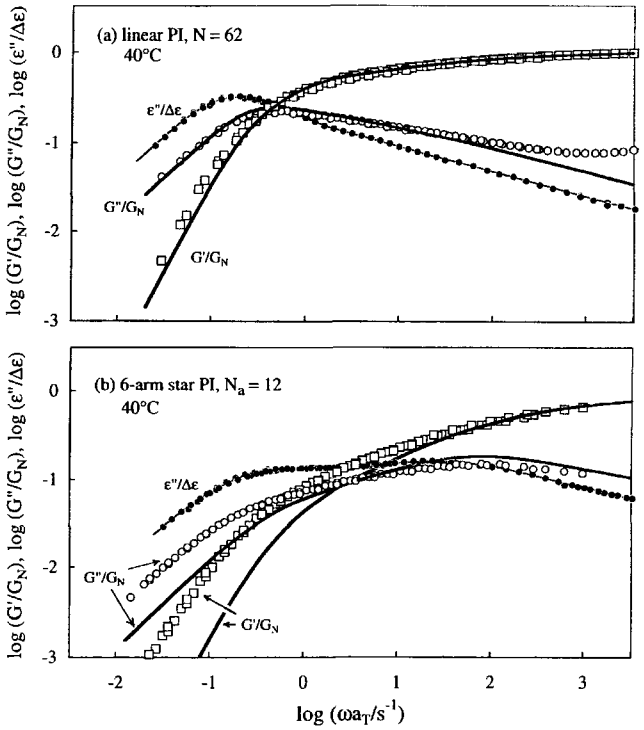

Fig. 6. Test of the simplest DTD relationship (in absence of the tube edge effect) for highly entangled linear and 6-arm star PI stars at 40°C. Filled circles indicate the normalized dielectric loss ($\varepsilon''/\Delta\varepsilon$) data, and thin curves represent the $\varepsilon''/\Delta\varepsilon$ recalculated from dielectric spectra. Normalized moduli data, G'/G_N (unfilled circles) and G''/G_N (filled circles), are compared with the moduli for the DTD process (thick curves) calculated from these spectra. The data were taken from Watanabe *et al.* (2001).

increasing N_a; cf. Fig. 5. Within the context of the tube model, this exponential retardation has been related to the *full* retraction of the star arm along the dilated tube (cf. Eqs. (17) and (18)). However, a detailed test of the DTD picture, conducted through comparison of the viscoelastic and dielectric data, poses a question for this assignment. The results of this test are summarized below.

4.2. test of DTD relationship

For highly entangled linear and star PI having nearly the same relaxation time $<\tau_e>_w$, the dielectric and viscoelastic behavior is compared in Fig. 6. The filled circles indicate the $\varepsilon''/\Delta\varepsilon$ data, and unfilled symbols represent the normalized moduli data.

If the entanglement mesh does not fluctuate with time (and the fixed-tube model is valid), G''/G_N (unfilled circles) should coincide with $\varepsilon''/\Delta\varepsilon$; Watanabe, 1999; Matsumiya *et al.*, 2000. However, this coincidence is not observed in Fig. 6, indicating that the tube moves/fluctuates even in the highly entangled monodisperse systems (with $N = 62$ and $N_a = 12$).

The DTD relationship derived *in absence of the tube-edge effect*, Eq. (14), can be easily tested for the data shown in Fig. 6. The viscoelastic DTD relaxation for a given $\Phi(t)$ is the slowest for $d = 1$, and the normalized moduli for this d are written in terms of the dielectric spectrum $\{g_p, \tau_p\}$ as

$$\frac{G'(\omega)}{G_N} = \omega^2 \sum_{p,k\geq 1} \frac{h_{pk}\tau_{pk}^2}{1+\omega^2\tau_{pk}^2}, \quad \frac{G''(\omega)}{G_N} = \omega \sum_{p,k\geq 1} \frac{h_{pk}\tau_{pk}}{1+\omega^2\tau_{pk}^2}$$

(for DTD with $d = 1$) (25)

with

$$h_{pk} = g_p g_k \text{ and } \tau_{pk} = [\tau_p^{-1} + \tau_k^{-1}]^{-1} \quad (26)$$

For the linear/star PI chains examined in Fig. 6, the dielectric spectra were evaluated from the $\varepsilon''/\Delta\varepsilon$ data with a previously reported iteration method (Yoshida *et al.*, 1989). The $\varepsilon''/\Delta\varepsilon$ recalculated from these spectra (thin curves) excellently coincides with the data (filled circles), indicating satisfactorily high accuracy of the spectra. The normalized moduli (Eq. (25)) calculated from these spectra are shown with the thick solid curves.

For the linear PI, the calculated moduli agree well with the data in the dominant part of terminal relaxation (at $\omega a_T < 10^3\ s^{-1}$), and the DTD picture in absence of the tube edge effect is valid; see Fig. 6a. In presence of this effect, the DTD relationship is modified to $\Phi(t) = \{\mu(t)\}^{1/(1+d)} - [\{\mu(t)\}^{-d/2(1+d)} - 1]^2/4N$ (cf. Eqs. (9) and (12)). However, the highly entangled linear PI chain exhibits narrow terminal viscoelastic mode distribution (as noted in Fig. 6a) and $\mu(t)$ does not significantly decay up to $t = <\tau_G>_w$. For this case, the second term of the modified relationship (~ $O(1/N)$) is negligible compared to the first term, and the calculated moduli were practically unaffected by the tube edge effect. Thus, for the linear PI with $N = 62$, the DTD picture (with/without tube edge effect) holds as a very good approximation. Similar success of this picture was found for the other linear PI chains examined in Fig. 3.

In contrast, for the star PI, the viscoelastic relaxation calculated for the DTD process with $d = 1$ is significantly *faster* than observed; see Fig. 6b. This result indicates the failure of the DTD picture (in absence of the tube edge effect) for the highly entangled star PI chains. (Remember that $d = 1$ gives the slowest possible DTD relaxation.) Differing from the situation for the linear PI, $\mu(t)$ of the star PI considerably decays at t well below $<\tau_G>_w$, and the tube edge effect changes the calculated moduli to a detectable extent. However, even with this effect, the calculated moduli did not agree with the data. Thus, for the star PI with $N_a = 12$, the DTD picture (with/without tube edge effect) failed in the dominant part of the terminal relaxation. Similar failure was found for the other star PI chains examined in Fig. 4.

The difference between the linear and star PI, the success

and failure of the DTD picture, is intimately related to the pre-requisite of this picture, the mutual equilibration of the successive entanglement segments through their constraint release (CR) motion. For the tube to be dilated to the diameter $a'(t)$, successive $\{a'(t)/a\}^2$ entanglement segments are required to be equilibrated within the time scale t. For the linear chain exhibiting narrow distribution of the relaxation modes, the expected dilation is just moderate even at $t \sim <\tau_G>_w$ so that the required CR-equilibration involves only a few segments. This equilibration can occur in time, and the tube actually dilates to the expected level, i.e., to $a' = a\{\varphi'(t)\}^{-d/2} \cong a\{\Phi(t)\}^{-d/2}$, as demonstrated in Fig. 6a.

In contrast, for the star chain having broadly distributed relaxation modes, the diameter $a'(t)$ expected at $t \sim <\tau_G>_w$ is considerably large and the CR-equilibration of $\{a'(t)/a\}^2$ segments cannot occur in time. This insufficient CR-equilibration results in the observed failure of the DTD picture.

4.3. comparison of data with DTD model

In this section, the failure of the DTD picture for the star chain is further examined in relation to the Milner-McLeish (MM) model formulated on the basis of this picture. For this model (with the tube edge effect), the normalized moduli and the dielectric constant/loss are obtained as the Fourier transformation of the $\mu(t)$ and $\Phi(t)$ given by Eqs. (19) and (21), respectively.

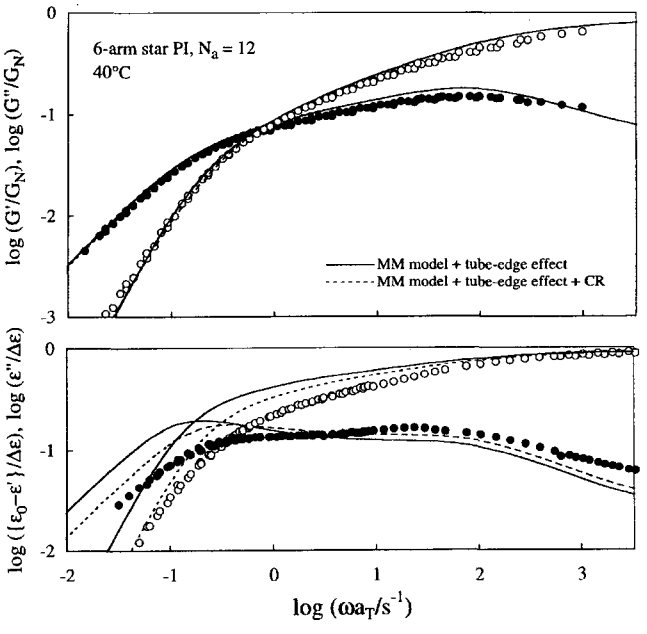

Fig. 7. Comparison of viscoelastic/dielectric data (circles) of highly entangled star PI chain ($N_a = 12$) with predictions of MM model in presence of the tube-edge effect (solid curves). Dotted curves represent the prediction of the DTD-CR model (= *MM* model modified through incorporation of the CR process). The data were taken from Watanabe *et al.* (2001).

In Fig. 7, the viscoelastic/dielectric properties calculated from the MM model (solid curves) are compared with the data (symbols) for the star PI with $N_a = 12$. The model parameter N_a was adjusted a little ($N_{a,cal} = 15$ instead of $N_a = 12$) to give the best agreement between the calculated and measured moduli, and the other parameter τ^* was chosen in a way that the calculated viscosity η_0 coincided with the data. With these choices of the parameters, the MM model excellently describes the moduli data including the high-ω G'' peak due to the Rouse-like fluctuation of the arm length; see top panel.

Nevertheless, the dielectric properties calculated from the *same* set of the parameters are significantly different from the data; see solid curves in the bottom panel of Fig. 7. Specifically, the calculated terminal dielectric relaxation time τ_ε is considerably longer than observed. This τ_ε remains the same even in absence of the tube-edge effect (cf. Eq. (20)). Thus, the terminal dielectric relaxation is not well described by the MM model with/without this effect.

A few comments should be added for this result. As seen in Fig. 6, the viscoelastic DTD relaxation calculated from the dielectric data (Eq. (14) with $d = 1$) is faster than observed. Consequently, the dielectric relaxation for the DTD process calculated from the viscoelastic data is slower than observed. This result is consistent with that seen in Fig. 7 (as readily expected from the approximate validity of Eq. (14) with $d = 1$ for the $\mu(t)$ and $\Phi(t)$ of the MM model.)

More importantly, in Fig. 7, the failure of the DTD picture incorporated in the model is noted only for the dielectric data. In other words, validity of this picture might have been concluded *if* we had examined only the viscoelastic data. It is the comparison of the viscoelastic and dielectric data (Figs. 6 and 7) that enabled us to resolve the detailed dynamic feature, the failure of the DTD picture for the star chain. This fact demonstrates the importance of this comparison.

4.4. DTD-CR model

For the star chain, the DTD picture is valid when the CR-equilibration is faster than the arm motion along the dilated tube. In the MM model, this arm motion is characterized with the relaxation time $\tau_{MM}(z)$ (Eq. (15)). Thus, the DTD formulation in this model is valid for the entanglement segments having $\tau_{MM}(z) > \tau^{**}(z)$ but a modification is required for those having $\tau_{MM}(z) < \tau^{**}(z)$, where $\tau^{**}(z)$ is the CR-equilibration time over $(1-z/L_{eq})^{-4/3}$ segments (included in the dilated tube segment of the diameter $a' = a(1-z/L_{eq})^{-2/3}$).

Following this molecular picture, we estimated the threshold z^{**} for crossover from the DTD picture ($z < z^{**}$) to the CR picture ($z > z^{**}$) and attempted to modify the MM model by simply incorporating the CR process for $z > z^{**}$. The aim of this modification is to examine the importance of the terminal CR process and explore a possible direction of the model refinement.

For this modified model hereafter referred to as *DTD-CR* model, $\mu(t)$ and $\Phi(t)$ are written as (Watanabe *et al.*, 2001)

$$\mu(t)=\frac{7}{3L_{eq}}\int_0^{z^{**}}\left[1-\frac{z}{L_{eq}}\right]^{4/3}\exp\left(-\frac{t}{\tau_{MM}(z)}\right)dz+I_{G,CR}\mu_{CR}(t) \quad (27)$$

$$\Phi(t)=\frac{1}{L_{eq}}\int_0^{z^{**}}\left[1+\frac{1}{6N_a}\left\{\left(1-\frac{z}{L_{eq}}\right)^{-7/3}-\left(1-\frac{z}{L_{eq}}\right)^{-5/3}\right\}\right]$$

$$\times\exp\left(-\frac{t}{\tau_{MM}(z)}\right)dz+I_{\varepsilon,CR}\Phi_{CR}(t \quad (28)$$

with

$$I_{G,CR}=\left(1-\frac{z^{**}}{L_{eq}}\right)^{7/3},\quad I_{\varepsilon,CR}=1-\frac{z^{**}}{L_{eq}}-\frac{1}{8N_a}\left\{1-\left(1-\frac{z^{**}}{L_{eq}}\right)^{-2/3}\right\}^2 \quad (29)$$

In both Eqs. (27) and (28), the first term indicates the relaxation due to the MM-type arm retraction over a distance z^{**}, and the second term represents the CR relaxation with the viscoelastic intensity $I_{G,CR}$ and/or dielectric intensity $I_{\varepsilon,CR}$. These intensities (Eq. (29)) were obtained by subtracting the viscoelastic/dielectric intensities for the MM retraction process (the first terms in Eqs. (27) and (28) at $t = 0$) from unity.

The normalized CR functions, $\mu_{CR}(t)$ and $\Phi_{CR}(t)$, were calculated from the Rouse-Ham equation for a q-arm bead-spring star-chain (Watanabe *et al.*, 2001). This equation mimics the chain motion due to accumulated local CR-hopping and gives characteristic distribution of the relaxation mode intensities: The viscoelastic intensities are the same for all Rouse-Ham modes (irrespective of the mode indices), and the odd modes activating anti-symmetric motion of a pair of arms are degenerated by a factor of q-1.

In contrast, the dielectric intensity of the Rouse-Ham mode rapidly decreases with increasing mode index, and Φ_{CR} is close to a single-mode function relaxing with the terminal time $\tau_{\varepsilon,CR}$. For the star PI having the dipole inversion at the branching point, this $\tau_{\varepsilon,CR}$ is given by the relaxation time $\tau_2^{(CR)}$ of the second-slowest CR mode because the anti-symmetric arm motion activated by the slowest mode induces no change in the polarization (Yoshida *et al.*, 1989; Watanabe *et al.*, 2001). This *dielectric extinction* of the slowest mode (and of higher order odd modes) is a characteristic feature of the Rouse-Ham type CR process of the star chains.

The $\mu(t)$ and $\Phi(t)$ of the DTD-CR model (Eqs. (27) and (28)) can be explicitly calculated if the DTD-CR threshold z^{**} and the relaxation time $\tau_1^{(CR)}$ of the slowest CR mode are known. ($\tau_2^{(CR)}$ is calculated from $\tau_1^{(CR)}$). These z^{**} and $\tau_1^{(CR)}$ were evaluated from Rouse-Ham analysis for the CR process explained in Appendix *C*. This analysis required a number of constraints per entanglement point, n_g, and the results obtained for $n_g = 1.5$ (giving the dielectric relaxation time close to the data) are shown below.

For the star PI chain examined in Fig. 7, the analysis gave $z^{**} = 0.84L_{eq}$ and $\tau_1^{(CR)} = 4\tau_{MM}(z^{**})$. Thus, the number of entanglement segments n_{CR} (per arm) involved in the terminal CR process and the terminal dielectric CR time $\tau_2^{(CR)}$ are estimated as

$$n_{CR}=N_a\left(1-\frac{z^{**}}{L_{eq}}\right)\cong 2 \quad (30)$$

$$\tau_2^{(CR)}=\left[\sin^{-2}\left(\frac{\pi}{2n_{CR}}\right)\sin^2\left(\frac{\pi}{2(2n_{CR}+1)}\right)\right]\tau_1^{(CR)}\cong 0.76\tau_{MM}(z^{**}) \quad (31)$$

(In Eq. (31), the pre-factor for $\tau_1^{(CR)}$ is a squared ratio of the first and second Rouse-Ham eigenvalues.) The viscoelastic and dielectric properties of the DTD-CR model calculated from these parameters are shown with the dotted curves in Fig. 7. The $N_{a,cal}$ value utilized in the calculation was the same as that for the original MM model ($N_{a,cal} = 15$), and the other parameter τ^* was chosen in a way that the η_0 calculated from the DTD-CR model coincided with the data.

As noted in the top panel of Fig. 7, the solid and dotted curves are almost indistinguishable and the incorporation of the CR process in the MM model hardly changes the model prediction for the moduli. This result reflects a fact that the initial modulus sustained by the segments at $z > z^{**}$ has mostly relaxed during the DTD process and only a small intensity $I_{G,CR}$ (= 0.014 for $z^{**} = 0.84L_{eq}$; cf. Eq. (29)) remains for the CR process of these segments. Thus, the CR process is hardly detectable for the viscoelastic moduli.

In contrast, the dielectric behavior is significantly affected by the CR process because a considerably large dielectric intensity $I_{\varepsilon,CR}$ (= 0.11 for $z^{**} = 0.84L_{eq}$; cf. Eq. (29)) remains for this process; see the bottom panel of Fig. 7. The calculated terminal dielectric relaxation is faster and the terminal intensity is smaller for the DTD-CR model (dotted curve) than for the MM model (solid curve), and the DTD-CR prediction appears to be in better agreement with the data. Specifically, the DTD-CR model (for n_g = 1.5) well describes the $\varepsilon''/\Delta\varepsilon$ peak frequency in the terminal regime.

For further comparison of the DTD-CR and MM models, Fig. 8a shows *experimentally detectable* longest relaxation times τ_{max} calculated from these models. These τ_{max} are normalized by τ^* (Rouse relaxation time in one entanglement segment) and plotted against $N_{a,cal}$.

For the MM model, the viscoelastic and dielectric τ_{max} are the same and given by $\tau_{MM}(L_{eq})$ (solid curve).

For the DTD-CR model, the rigorously defined *viscoelastic* τ_{max} is given by $\tau_1^{(CR)}/2$ (Watanabe *et al.*, 2001). However, the CR process has a very small viscoelastic intensity $I_{G,CR}$ and should be hardly detectable in experi-

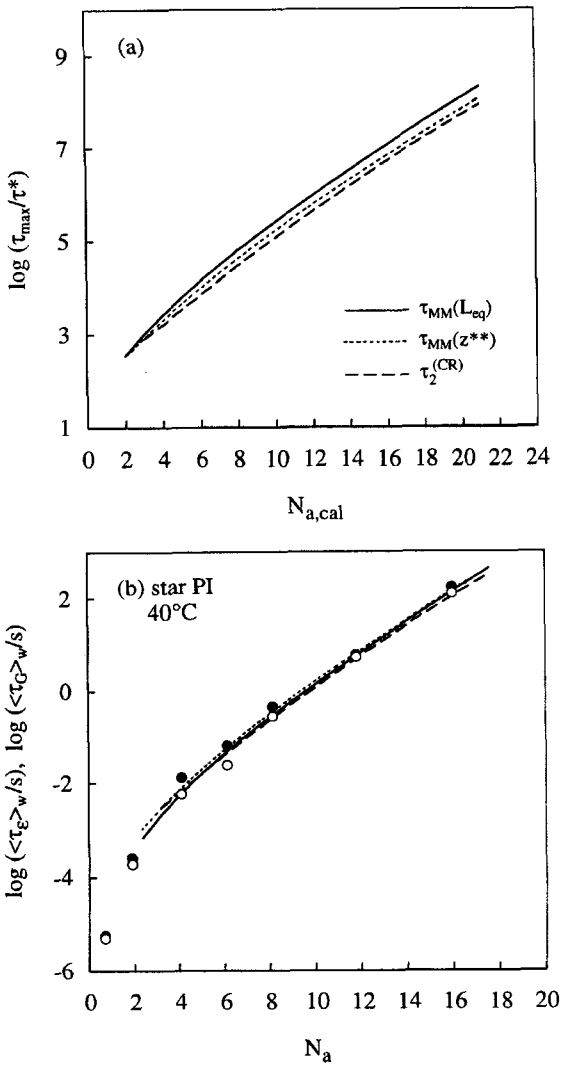

Fig. 8. (a) $N_{a,cal}$ dependence of the experimentally detectable longest relaxation time τ_{max} predicted from the MM and DTD-CR models. (b) Comparison of the MM and DTD-CR predictions (curves) with the terminal relaxation times of 6-arm star PI chains, $<\tau_\varepsilon>_w$ (unfilled circles) and $<\tau_G>_w$ (filled circles). In the comparison, the arm length in the models was a little adjusted ($N_{a,cal} = 5N_a/4$), and the Rouse relaxation time in one entanglement segment τ^* was chosen to achieve the best agreement of the prediction and experiments. The data were taken from Yoshida *et al.* (1989) and Watanabe *et al.* (2000, 2001).

ments. Thus, the detectable viscoelastic τ_{max} is given by $\tau_{MM}(z^{**})$ required for the retraction over the distance z^{**} (dotted curve).

In contrast, the terminal CR process of the DTD-CR model has a sufficiently large dielectric intensity $I_{\varepsilon,CR}$. Thus, the detectable dielectric τ_{max} should coincide with $\tau_2^{(CR)}$ of the second-slowest CR mode (dashed curve). (Remember that the slowest CR mode is dielectrically inert.) This $\tau_2^{(CR)}$ is fairly close to the viscoelastic $\tau_{MM}(z^{**})$, meaning that the coincidence of the viscoelastic and dielectric τ_{max} seen for the MM model is not significantly altered in the DTD-CR model.

Fig. 8a also demonstrates that the $\tau_{MM}(L_{eq})$, $\tau_{MM}(z^{**})$, and $\tau_2^{(CR)}$ exhibit almost indistinguishable, exponential $N_{a,cal}$ dependence. Thus, the DTD-CR model can describe the N_a dependence of the $<\tau_\varepsilon>_w$ and $<\tau_G>_w$ data (Fig. 5) with the accuracy similar to that for the MM model. In fact, Fig. 8b demonstrates good agreement between the data (symbols) and the model predictions (curves) with a little adjustment of $N_{a,cal}$ ($= 5N_a/4$).

From this agreement as well as the moderate improvement of the prediction for the dielectric behavior by incorporation of the CR process (Fig. 7), the combination of the DTD and CR processes appears to be essential for accurate description of the star chain dynamics, although the combination in the above DTD-CR model (simple addition of the DTD and CR functions) is crude and further refinement is required.

5. Concluding Remarks

For highly entangled linear and star PI chains having the type-A dipoles, we have examined the linear viscoelastic and dielectric properties within the context of the tube model considering the DTD and CR processes. Comparison of these properties indicated that the DTD picture is valid for the linear chains but fails for the star chains in the dominant part of the terminal relaxation. This result, found irrespective of the tube-edge effect on the dielectric behavior, suggests that the CR mechanism has a significant contribution to the terminal relaxation of the star chains.

On the basis of this result, we have modified the tube model (MM model) by incorporating the CR process. This modification was made by simply adding the DTD and CR relaxation functions (the latter being defined only for the segments near the branching point). This crude modification moderately improved the model prediction for the dielectric behavior. Refinement of the model, achieved by self-consistent combination of the CR and DTD processes, is an important subject of future work.

It should be emphasized that the viscoelastic and dielectric properties differently average the same stochastic chain motion and this difference enabled us to resolve detailed dynamic features explained above. Comparison of various different properties (including optical and diffusion properties) will be very useful in further investigation of polymer chain dynamics.

Acknowledgments

The work summarized in this review was partly supported by the Ministry of Education, Culture, and Sports, Science, and Technology, Japan (grant No. 12650884) and

by Japan Chemical Innovation Institute (through the Doi Project for development of Platform for designing high functional materials).

Appendix A. Modulus decay due to dynamic tube dilation

The normalized modulus decays when the tube dilates. To calculate this decay, we apply the general modulus expression, Eq. (1), to successive β entanglement segments of the chain (indexed with $n = j\beta + 1, j\beta + 2, .., (j+1)\beta$). If these β segments are in the dilated tube and mutually equilibrated (randomized) through their CR motion in the time scale of t while keeping a vectorial sum $\boldsymbol{u}'(0)$ of their bond vectors at the time 0, the bond vectors at the time t can be written as (Watanabe, 1999, 2001)

$$\boldsymbol{u}(n,t) = \frac{1}{\beta}\boldsymbol{u}'(0) + \boldsymbol{v}(n,t) \quad \text{for } n = (i-1)\beta + 1, \; (i-1)\beta + 2, \; ..., \; i\beta \tag{32}$$

Here, $\boldsymbol{v}$ is an isotropically distributed vector uncorrelated with $\boldsymbol{u}'$. Then, we obtain (cf. Eq. (1))

$$\mu_\beta(t) = \frac{1}{S_0 N}\sum_{n=j\beta+1}^{j\beta}\frac{1}{a^2}\langle u_x(n,t)u_y(n,t)\rangle = \frac{1}{S_0 N}\frac{1}{\beta a^2}\langle u'_x(0)u'_y(0)\rangle \tag{33}$$

Under the affine deformation condition, the initial orientational anisotropy is the same for Gaussian segments of any size; namely, $< u_x(n,0)u_y(n,0)>/a^2 = < u'_x(0)u'_y(0)>/\beta a^2 = S_0 = \gamma/3$; cf. Eq. (3). (Note that the average size of the β segments as a whole is given by βa^2.) Thus, Eq. (33) gives $\mu_\beta(t) = 1/N$. This $\mu_\beta(t)$ value is smaller, by a factor of $1/\beta$, than the initial value, $\mu_\beta(0) = \beta/N$ (cf. Eq. (33) with $<u_x u_y>/a^2 = S_0$). Namely, the DTD process resulting from the CR-equilibration over β segments leads to a decay of the modulus by the factor of $1/\beta$. (In other words, the CR-equilibrated β segments together behave as an enlarged modulus-sustaining unit.)

Appendix B. Segment displacement in tube-edge plane

The displacement in the edge-plane of the surviving portion of the dilated tube has the maximum effect on the dielectric $\Phi(t)$ when the chain in this portion (cf. Fig. 2) is fully equilibrated in both length and orientation. For this case, we find a relationship

$$\langle \boldsymbol{D}(t)\cdot\boldsymbol{R}_{in}(0)\rangle = \langle \boldsymbol{D}'(t)\cdot\boldsymbol{R}_{in}(0)\rangle = -\frac{1}{2}\langle\{\boldsymbol{D}(t)\}^2\rangle \tag{34}$$

(Eq. (34) is derived from an identity $<\{\boldsymbol{R}_{in}(t)\}^2> = <\{\boldsymbol{R}_{in}(0)\}^2>$ valid in the fully equilibrated state).

The mean-square displacement $<\{\boldsymbol{D}(t)\}^2>$ appearing in Eq. (34) can be evaluated as an integral in the edge-plane of the dilated tube (designated as a ξ-η plane),

$$\langle\{D(t)\}^2\rangle = \frac{1}{\pi^2(a'/2)^4}\int\{(\xi-\xi_0)^2+(\eta-\eta_0)^2\}d\xi d\xi_0 d\eta d\eta_0 = \left(\frac{a'-a}{2}\right)^2 \tag{35}$$

Here, (ξ, η) and (ξ_0, η_0) indicate the coordinates of the edge segment at times t and 0, and the integral is conducted in a circular region of diameter a'–a (available for the center of mass of the edge-segment). From Eqs. (34) and (35) together with the expression of the dilated tube diameter, $a' = a\{\varphi'(t)\}^{-d/2}$, Eq. (10) is rearranged to Eq. (12).

Appendix C. Analyses of DTD-CR threshold and slowest CR time

For linear chains, the Graessley model (assuming the Rouse-CR dynamics) calculates a local entanglement lifetime t_w as a mean waiting time for first removal of constraint due to motion of surrounding chains (Graessley, 1982). For the star arm exhibiting the DTD-CR crossover, this removal would be dominated by the MM-type retraction of an entangling partner segment (if the partner's coordinate y is smaller than the DTD-CR threshold z^{**}) or by the local CR-hopping of this partner (if $y > z^{**}$). Thus, extending Graessley's calculation to the star arm, we estimated the t_w as (Watanabe *et al.*, 2001)

$$t_w = \int_0^\infty \{F(t)\}^{n_g} dt \quad \text{with}$$

$$F(t) = \frac{1}{L_{eq}}\int_0^{z^{**}} \exp\left(-\frac{t}{\tau_{MM}(y)}\right)dy + \left\{1-\frac{z^{**}}{L_{eq}}\right\}\exp\left(-\frac{t}{t_w}\right) \tag{36}$$

Here, the first and second terms of $F(t)$ correspond to the constraint removal due to the MM-type retraction and CR hopping, respectively. The n_g represents a number of constraints per entanglement point (Graessley, 1982). In the actual calculation, we chose $n_g = 1.5$ giving the dielectric relaxation time close to the data.

In evaluation of z^{**}, we firstly assumed various DTD-CR threshold values z' and numerically solved Eq. (36) to calculate $t_w(z')$ for respective z' values (Watanabe *et al.*, 2001). From this $t_w(z')$, the CR-equilibration time over $(1 - z'/L_{eq})^{-4/3}$ segments was evaluated as the discretized Rouse-CR orientational relaxation time, $\tau^{**}(z') = 0.5t_w(z') \sin^{-2}\{\pi/2\beta(z')\}$ with $\beta(z') = (1 - z'/L_{eq})^{-4/3}$. This $\tau^{**}(z')$ was compared with $\tau_{MM}(z')$ in the entire range of z' to determine the correct threshold value z^{**} satisfying a DTD-CR crossover relationship $\tau^{**}(z^{**}) = \tau_{MM}(z^{**})$. From this z^{**} value, the number of entanglement segments (per arm) involved in the terminal CR process was evaluated to be $n_{CR} = N_a(1 - z^{**}/L_{eq})$.

The slowest Rouse-Ham CR mode corresponds to the CR-hopping of $2n_{CR}$ segments (in two arms) with the mean waiting time t_w, and its relaxation time is given by (Watanabe *et al.*, 2001)

$$\tau_1^{(CR)} = t_w \sin^{-2}\left(\frac{\pi}{2(2n_{CR}+1)}\right)$$

(discretized Rouse-Ham expression) (37)

However, this slowest CR mode can be activated only after the star arm retracts along the dilated tube by the distance z^{**}. (In absence of this retraction, the n_{CR}-th segment in each arm is effectively bound in the dilated tube and its CR-motion over a distance $a' = a(1 - z^{**}/L_{eq})^{-2/3}$ is suppressed.) The CR time governed by this retraction-controlled hopping is written as (Watanabe *et al.*, 2001)

$$\tilde{\tau}_1^{(CR)} = 4\tau_{MM}(z^{**}) \quad (38)$$

The actual terminal CR relaxation occurs through competition of the accumulation of the local-CR hopping and the arm retraction over the distance z^{**} (pre-requisite of the terminal CR): This relaxation occurs at $\tau_1^{(CR)}$ if $\tilde{\tau}_1^{(CR)} < \tau_1^{(CR)}$ and at $\tilde{\tau}_1^{(CR)}$ if $\tilde{\tau}_1^{(CR)} > \tau_1^{(CR)}$. Thus, we compared the $\tau_1^{(CR)}$ and $\tilde{\tau}_1^{(CR)}$ to determine the actual CR time. For the local constraint number $n_g = 1.5$ (utilized in the above calculation of z^{**}), we found that $\tilde{\tau}_1^{(CR)} > \tau_1^{(CR)}$ for the stars with large N_a and the terminal CR time is given by $\tilde{\tau}_1^{(CR)}$ (Eq. (38)).

References

Ball, R. C. and T. C. B. McLeish, 1989, Dynamic dilution and the viscosity of star polymer melts, *Macromolecules* **22**, 1911-1913.

Bartles, C. R., B. Crist, L. J. Fetters, and W. W. Graessley, 1986, Self-diffusion in branched polymer melts, *Macromolecules* **19**, 785-793.

Doi, M. and S. F. Edwards, 1978, Dynamics of concentrated polymer systems. part 2. molecular motion under flow, *J. Chem. Soc. Faraday Trans. 2* **74**, 1802-1817.

Doi, M. and S. F. Edwards, 1986, The Theory of Polymer Dynamics, Clarendon, Oxford.

Ferry, J. D., 1980, Viscoelastic Properties of Polymers (3rd ed), Wiley, New York.

Fetters, L. J., A. D. Kiss, D. S. Pearson, G. F. Quack, and F. J. Vitus, 1993, Rheological behavior of star-shaped polymers, *Macromolecules* **26**, 647-654.

Graessley, W. W., 1982, Entangled linear, branched and network polymer systems - molecular theories, *Adv. Polym. Sci.* **47**, 67-117.

Janeschitz-Kriegl, H., 1983, Polymer melt rheology and flow birefringence, Springer, Berlin.

Klein, J., 1978, The onset of entangled behavior in semidilute and concentrated polymer solutions, *Macromolecules* **11**, 852-858.

Lantman, C. W., J. F. Tassin, L. Monnerie, L. J. Fetters, E. Helfand, and D. S. Pearson, 1989, Fourier transform infrared dichroism study of orientation relaxation using isotropically labeled polystyrene stars, *Macromolecules* **22**, 1184-1188.

Marrucci, G., 1985, Relaxation by reptation and tube enlargement: a model for polydisperse polymers, *J. Polym. Sci., Polym. Phys. Ed.* **23**, 159-177.

Matsumiya, Y., H. Watanabe, and K. Osaki, 2000, Comparison of dielectric and viscoelastic relaxation functions of cis-polyisoprenes: test of tube dilation molecular picture, *Macromolecules* **33**, 499-506.

Matsumiya Y. and H. Watanabe, 2001, Further test of the tube dilation process in star-branched cis-polyisoprene: role of branching-point fluctuation, *Macromolecules* **34**, 5702-5710.

Milner, S. T. and T. C. B. McLeish, 1997, Parameter-free theory for stress relaxation in star polymer melts, *Macromolecules* **30**, 2159-2166.

Milner, S. T. and T. C. B. McLeish, 1998, Arm-length dependence of stress relaxation in star polymer melts, *Macromolecules* **31**, 7479-7482.

Pearson, D. S. and E. Helfand, 1984, Viscoelastic properties of star-shaped polymers, *Macromolecules* **17**, 888-895.

Riande, E. and E. Saiz, 1992, Dipole Moments and Birefringence of Polymers, Prentice Hall, Englewood Cliffs (NJ, USA).

Shull, K. R., E. J. Kramer, G. Hadziioannou, M. Antonietti, and H. Sillescu, 1988, Diffusion of macromolecular stars in linear, microgel, and network matrices, *Macromolecules* **21**, 2578-2580.

Tassin, J. F., L. Monnerie, and L. J. Fetters, 1988, Infrared dichroism study of the relaxation of selected segments along a stretched polymer chain and comparison with theoretical models, *Macromolecules* **21**, 2404-2412.

Watanabe, H., M.-L. Yao and K. Osaki, 1996, Comparison of dielectric and viscoelastic behavior of polyisoprene solutions: coherence in subchain motion, *Macromolecules* **29**, 97-103.

Watanabe, H., Y. Matsumiya, K. Osaki, and M.-L. Yao, 1998, Dynamics of dipole-inverted cis-polyisoprene chains in a matrix of long, entangling chains. 2. effects of constraint release on the coherence of the subchain motion, *Macromolecules* **31**, 7538-7545.

Watanabe, H., 1999, Viscoelasticity and dynamics of entangled polymers, *Prog. Polym. Sci.* **24**, 1253-1403.

Watanabe, H., Y. Matsumiya, and K. Osaki, 2000, Tube dilation process in star-branched cis-polyisoprenes, *J. Polym. Sci. Part B Polym. Phys.* **38**, 1024-1036.

Watanabe, H., 2001, Dielectric relaxation of type-A polymers in melts and solutions, *Macromol. Rapid Commun.* **22**, 127-175.

Watanabe, H. and Y. Matsumiya, 2001a, Dielectric and viscoelastic properties of star-branched cis-polyisoprene: test of tube dilation mechanism, *Proceedings of ICAPP2001 Yonezawa*, in press.

Watanabe, H., Y. Matsumiya, and T. Inoue, 2001b, Dielectric and viscoelastic relaxation of highly entangled polyisoprene stars: quantitative test of tube dilation model, *Macromolecules*, in press.

Ylitalo, C. M., G. G. Fuller, V. Abetz, R. Stadler, and D. S. Pearson, 1990, Relaxation dynamics of selected polymer chain segments and comparison with theoretical models *Rheol. Acta* **29**, 543-555.

Yoshida, H., K. Adachi, H. Watanabe, and T. Kotaka, 1989, Dielectric normal mode process of star-shaped polyisoprenes, *Polymer J.* **21**, 863-872.